
Article:
Yang, Y., Ahmed, B., Mitchell, C. et al. (2021) Investigation of wet milling and indirect ultrasound as means for controlling nucleation in the continuous crystallization of an active pharmaceutical ingredient. Organic Process Research & Development, 25 (9). pp. 2119-2132. ISSN: 1083-6160

https://doi.org/10.1021/acs.oprd.1c00209

ORGANIC PROCESS RESEARCH & DEVELOPMENT
OPR&D

pubs.acs.org/OPRD

Article

Investigation of Wet Milling and Indirect Ultrasound as Means for Controlling Nucleation in the Continuous Crystallization of an Active Pharmaceutical Ingredient

Yihui Yang,* Bilal Ahmed, Christopher Mitchell, Justin L. Quon, Humera Siddique, Ian Houson, Alastair J. Florence,* and Charles D. Papageorgiou

Cite This: *Org. Process Res. Dev.* 2021, 25, 2119–2132

Read Online

ACCESS | Metrics & More | Article Recommendations

ABSTRACT: This study compares the use of wet milling and indirect ultrasound for promoting nucleation and controlling the particle size during the continuous crystallization of a hard-to-nucleate active pharmaceutical ingredient (API). Both an immersion and an external wet mill installed on a recirculation loop were investigated. It was found that all methodologies significantly improved the nucleation kinetics, and the effects of key process parameters (*e.g.*, mill speed, temperature, and ultrasound intensity) on particle size were experimentally investigated. A minimum d_{50} of 27 and 36.8 μm was achieved when using the wet mill and ultrasound, respectively. The effectiveness of wet milling was demonstrated in a three-stage mixed suspension mixed product removal continuous crystallization of the API that was operated continuously for 12 h (eight residence times), achieving a steady state with minimal fouling. Strategies for improving the overall robustness of the setup in routine manufacturing are discussed.

KEYWORDS: *wet milling, ultrasound, continuous crystallization, fouling, mixed suspension mixed product removal crystallizer, crystallization*

1. INTRODUCTION

Continuous manufacturing of active pharmaceutical ingredients (APIs) offers an attractive route for producing high-quality and consistent materials and reducing the time-to-market of newly discovered drugs. The majority of pharmaceutical products are delivered through oral solid dosage forms which require tight control of the crystalline material in terms of its purity and particle attributes (size and overall size distribution, shape, and form).[1] These attributes can be controlled from the crystallization unit operation which is an essential separation and purification technique used in small-molecule drug substance (DS) manufacturing.[2] Continuous crystallization has gained increasing interest from both the pharmaceutical industry and regulatory authorities, its benefits having been demonstrated on several APIs using different reactor types [*e.g.*, mixed suspension mixed product removal (MSMPR) and plug flow].[3−9] These include steady-state operation,[10] higher yield,[11,12] better control over crystallization mechanisms (supersaturation, nucleation, and crystal growth),[13] enhanced particle attributes (*e.g.*, size distribution),[14] increased heat transfer, and ease of scale-up.[15] The preferred reactor types used to achieve the aforementioned benefits are single- and multiple-stage MSMPR crystallizers primarily due to their ability to robustly handle solids and the flexibility they offer in process design allowing, for example, the use of readily available stirred tank reactors both at the lab and pilot scale.[16]

Crystallization process development involves selection of an appropriate solvent system,[17] a method to generate supersaturation (*e.g.*, cooling, antisolvent addition, evaporation, or pH adjustment),[18−21] and tuning of process parameters (*e.g.*, mixing intensity, cooling profile, antisolvent addition method and rate, and so forth) to achieve the desired crystal properties.[22,23] However, limited choices with solvent selection driven by upstream demands (*e.g.*, compatibility with reagents) often result in difficulty in controlling the interplay of the various crystallization mechanisms (agglomeration, attrition, breakage, encrustation, *etc.*,).[24,25] To mitigate these issues, particularly, where drug product performance-related attributes (*e.g.*, particle size and shape) cannot be delivered, alternative particle engineering strategies have been investigated, often using the application of external fields. Two such examples are ultrasound and high-shear rotor-stator technologies.

The main interest in applying ultrasound technology is for inducing nucleation at low supersaturations while manipulating the particle size and shape.[26] This can be achieved through the application of acoustic energy, resulting in cavitation generated from a probe horn (sonoprobe) typically placed in direct contact with the process solution.[27] Such an approach poses some significant limitations, for example, surface erosion leading to particle shedding and heavy metal contamination

Received: June 2, 2021
Published: September 1, 2021

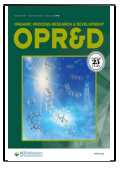

https://doi.org/10.1021/acs.oprd.1c00209
Org. Process Res. Dev. 2021, 25, 2119–2132

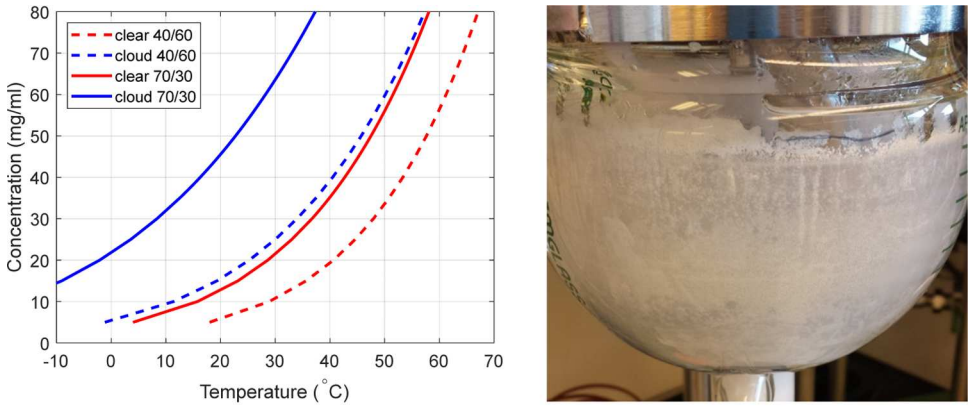

Figure 1. (a) Metastable zone for the two different solvent compositions investigated; (b) reactor fouling when the 40/60 v/v % MeOH/H_2O solvent system was used.

of the process stream,[27,28] substantial temperature deviations causing particle dissolution[29] and potential compound degradation, rapid dissipation of energy transferred per unit volume, and excessive noise in the vicinity of the probe leading to operator health and safety concerns.[30] An alternative and more attractive strategy would be to separate the sonoprobe from the process solution and use air or some other media to transfer the acoustic energy to the process medium (herein referred to as indirect sonication). However, there are few reports of this mode of application in the literature,[31,32] and it is unknown whether such a configuration can exert sufficient and consistent power transfer to influence the crystallization kinetics and particle attributes in a controllable manner.

On the other hand, high-shear rotor-stator wet milling devices have found widespread use in pharmaceutical manufacturing owing to their ease of use and broad availability. They can be applied either immersed into the reactor or through a recirculation loop to perform size reduction,[33−36] shape manipulation,[37−39] polymorphic selection,[40,41] conglomerate separation[42] in full-scale manufacturing,[43,44] or seed generation.[45,46] In continuous manufacturing, a key driver for applying wet milling is to control nucleation for APIs possessing wide metastable zone widths (MSZWs) and thus exhibiting slow nucleation kinetics. Its use has also been shown to reduce the process startup and time to reach the steady state.[47] For such APIs, control of nucleation or use of seed is critical to ensure a robust continuous process, maintain a steady state, and control encrustation and classification, which could result from supersaturation buildup and excessive particle growth resulting from the lack of the available surface area. While wet milling can be deployed as a continuous seed generator and potentially remove the need for external seeding,[47] understanding operational challenges such as process integration, robustness during extended continuous operation, and the particle size limits achievable remains unreported.

The API used in this study is discovered at Takeda Pharmaceuticals. The current crystallization process does not use seed as there are no known polymorphs and particle size control is achieved through a subsequent jet-milling process. The crude API is dissolved in a mixture of 40/60 v/v % MeOH/H_2O (15 vol) at 65 °C, and activated charcoal (3 wt %) is added to clarify the solution. The suspension is filtered, and the resulting solution is cooled to 5 °C over 5 h to crystallize the API. Particles with a typical d_{50} of around 200 μm are isolated in 90% yield (on an 85 kg scale), which are jet-milled to a d_{50} target of 2.5−11.0 μm. The objective of the work described in this manuscript is to develop a continuous crystallization process to control the particle size distribution (PSD) and avoid the additional milling step. Preliminary batch crystallization experiments suggested that the API exhibited slow nucleation kinetics but very good growth. Furthermore, MSZW experiments using Crystal 16 showed that the system held supersaturation very well (Figure 1a). Initial unseeded single-stage continuous crystallization experiments resulted in nucleation on/near the reactor wall, which was 3−5 °C lower in temperature than the process temperature, which lead to extreme fouling (Figure 1b) and failure to achieve the steady state. In order to minimize encrustation, the solvent composition was switched from 40/60 v/v % MeOH/H_2O to 70/30 v/v % MeOH/H_2O, in which the API had a wider MSZW. It was postulated that a wider MSZW would reduce the fouling on the reactor walls caused by the temperature difference between the solution and the walls. However, while improved, fouling was still observed over time and attempts to improve nucleation rates by increasing shear through increasing the MSMPR agitation rates, impeller design (retreat curve, pitch blade, and Rushton turbine), and material of construction (PTFE, SS) were unsuccessful. While the challenges with controlling nucleation could be controlled *via* a continuous seeded process, this would add further complexity in terms of process design, management of a separate raw material source, and obtaining seed of a small-enough particle size to afford the product with the target PSD (submicron/micron size seed would be required). Therefore, *in situ* strategies were investigated, and the results are described in this manuscript. Initially, experimental strategies using high shear wet milling and sonication are introduced where three different intensified approaches are investigated and the influence of key processing parameters on nucleation and particle properties is presented. From analysis of the process trends and operating conditions, wet milling was selected and integrated in a three-stage continuous MSMPR system that was operated for 16 h to produce the API.

2. EXPERIMENTAL SECTION

2.1. General Procedure for Wet Milling Experiments.

Piping and instrumentation diagrams (P&IDs) of a single-stage

https://doi.org/10.1021/acs.oprd.1c00209
Org. Process Res. Dev. 2021, 25, 2119−2132

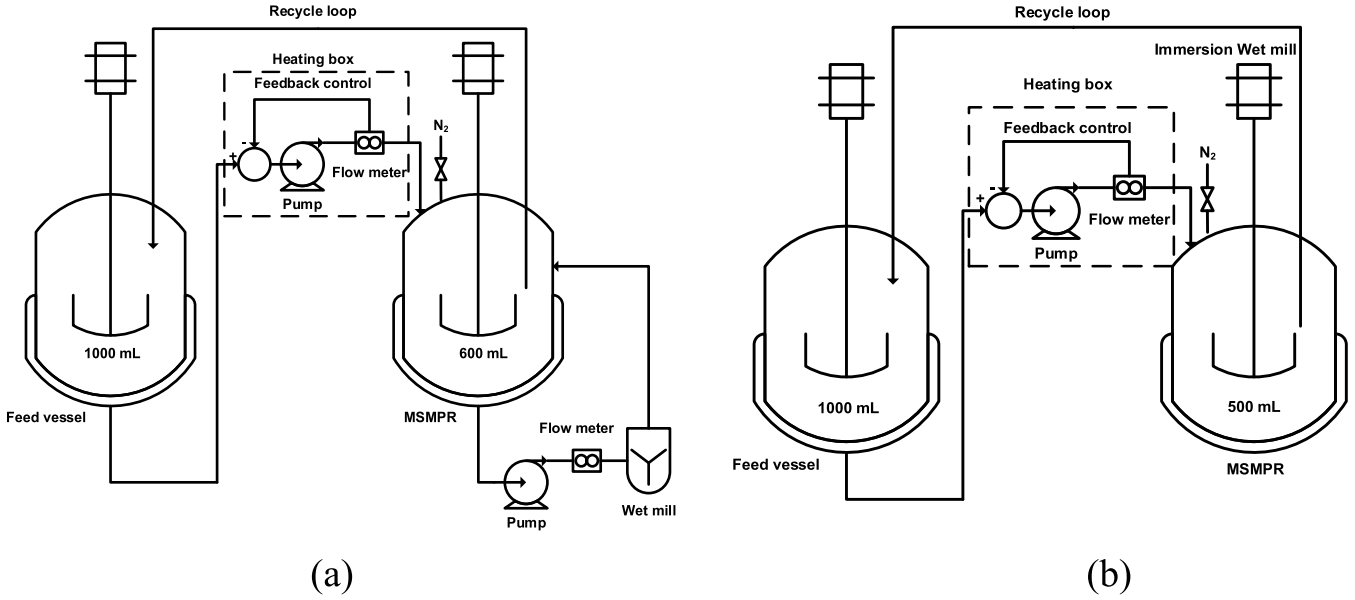

Figure 2. PI&Ds for the single-stage MSMPR/wet mill setup: (a) with an external wet mill and (b) with an immersion mill.

MSMPR setup equipped with both an external wet mill and an immersion mill are shown in Figure 2.

Two 1 L cylindrical jacketed vessels equipped with an overhead stirrer, a glass retreat curve impeller (three-blade, 68 mm diameter), temperature probe, and condensers were used as the feed tank and MSMPR crystallizer. A feedback flow rate control system based on a Red Lion programmable logic controller (PLC) and consisting of a gear pump (Ismatec, part number: ISM895E) and Coriolis flow meter (Bronkhorst, part number: M13-RGD-11-0-S) was used to transfer the hot solution (typically maintained at 55 °C) from the feed tank to the MSMPR. Both the gear pump and Coriolis flow meter were placed in an enclosed heating box maintained at 65 °C using an air heat blower (MISUMI, part number: MAHY-1310) to prevent the feed from crystallizing during the transfer.

For the experiments that used the external wet mill (IKA magic LAB), the flow rate through the mill was controlled and monitored using a Masterflex peristaltic pump (Masterflex L/S equipped with the pump head part number: 77390-00) and Coriolis flow meter (Bronkhorst, part number: M15-MAD-22-0-S) installed as part of the external recirculation loop. The pump was placed between the reactor and the flow meter, before the wet mill (Figure 2a). However, it was subsequently removed, as it was demonstrated that, across the ranges investigated, the flow rate through the wet mill (turnover number per residence) had only a small impact on the PSD (Figure 7b). 1/4″ OD PTFE tubing was used that was insulated with fiberglass to avoid heat loss. The wet mill was equipped with three fine generators and was heated to 40 °C using a thermocirculator (Huber Ministat 230).

The slurry transfer was achieved using a 1/4″ OD PTFE dip tube and pressurizing the MSMPR intermittently to 4 psi using nitrogen. A Siemens PLC was used to control the nitrogen valve and ensure that less than 10% of the total volume of the MSMPR was transferred each time in order to maintain a periodic steady state.[48] This resulted in transfers taking place every 3 min when the residence time was 30 min. To conserve the material, the suspension from the MSMPR was recycled and transferred directly back to the feed tank where it was dissolved and reused.

In a typical experiment, API (70 g, 152 mmol) and a 70/30 v/v % MeOH/H_2O solvent mixture (1 L, 14.3 vol) were charged to the feed tank and agitated at 250 rpm at 65 °C (10 °C above the saturation temperature) until fully dissolved. The API (42 g, 91 mmol) was then charged to the MSMPR crystallizer followed by a 70/30 v/v % MeOH/H_2O solvent mixture (0.6 L, 14.3 vol). The agitation speed was set to 250 rpm, and the suspension in the MSMPR was adjusted to the desired experimental temperature and maintained at that temperature for at least 30 min, until stable.

The external wet mill, if used, was switched on and set to the desired rotational speed. The Masterflex pump was switched on, and the desired flow rate was set using the Red Lion PLC. The suspension was recirculated through the mill for a minimum of 30 min until a constant particle size distribution was achieved, as indicated by the focused beam reflectance measurement (FBRM). The feed pump and Siemens PLCs were then turned on and set to the desired settings to transfer the feed solution to the MSMPR crystallizer and back to the feed vessel. The thermocirculator connected to the wet mill was set to the same temperature as the MSMPR crystallizer.

For the experiments employing an immersion mill, a special pressure-rated dispersing unit (part number: S25 KV) was used with the IKA T25 drive to allow for the use of pressure during the slurry transfer from the MSMPR. As shown in Figure 2b, in this setup, the overhead agitator was replaced with the mill, which was found to provide vigorous mixing across the agitation speeds and fill volumes investigated.

2.2. Three-Stage Continuous MSMPR Experimental Procedure. The P&ID of the three-stage MSMPR setup is shown in Figure 3a. One 3 L and three 1 L cylindrical jacketed vessels equipped with an overhead stirrer, a glass retreat curve impeller (three-blade, 68 mm diameter), temperature probe, and condensers were used as the feed tank and MSMPR crystallizers, respectively. The temperature of each reactor was independently controlled using a dedicated thermocirculator (Huber, Ministat 230). The configuration of the feed vessel and first stage of the MSMPR was identical to that shown in Figure 2a and described earlier. The only modification was that the return line from the wet mill to the reactor was heated to

https://doi.org/10.1021/acs.oprd.1c00209
Org. Process Res. Dev. 2021, 25, 2119−2132

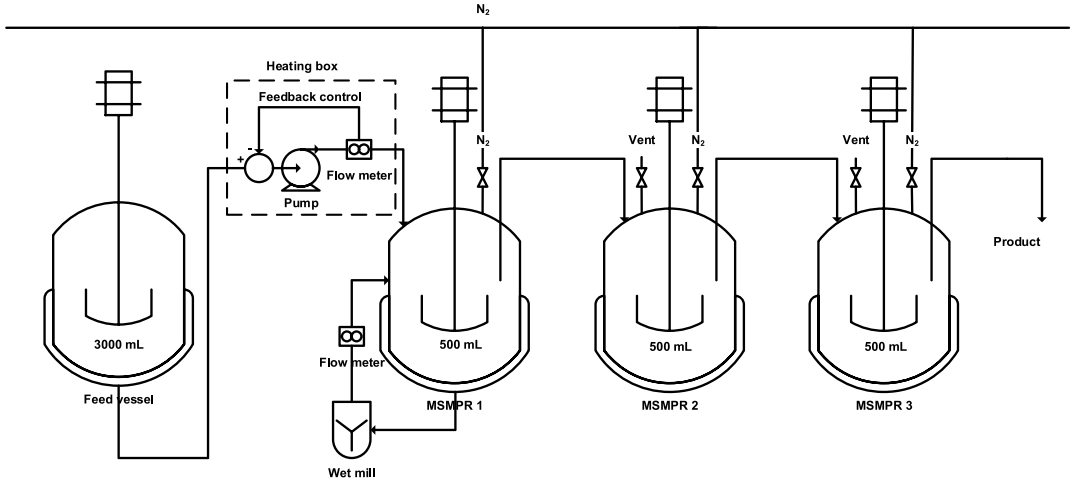

(a)

(b)

Figure 3. Three-stage MSMPR setup: (a) P&ID and (b) picture of the setup.

minimize fouling that was observed during the earlier optimization experiments.

API (210 g, 455 mmol) and a 70/30 v/v % MeOH/H_2O solvent mixture (3 L, 14.3 vol) were charged to the feed tank and agitated at 250 rpm at 65 °C (10 °C above the saturation temperature) until fully dissolved. The API (35 g, 76 mmol) was then charged to each of the three MSMPR crystallizers followed by a 70/30 v/v % MeOH/H_2O solvent mixture (0.5 L, 14.3 vol). The removal dip pipes were set to maintain the internal volume of each crystallizer at 0.5 L. The agitation speed was set to 250 rpm, and each stage was adjusted to the desired experimental temperature and maintained at that temperature for at least 30 min, until stable (45, 35, and 5 °C for stages 1, 2, and 3, respectively).

The external wet mill equipped with three fine rotors was set to 12,400 rpm. The suspension was recirculated for 30 min until a constant particle size distribution was achieved, as indicated by the FBRM. The feed pump and Siemens PLCs were then turned on and set to 16.67 mL/min to maintain a total system residence time of 90 min (30 min in each of the three stages). The thermocirculator connected to the wet mill was set to 40 °C in order to maintain the temperature of the stage 1 crystallizer at 45 °C. The product from the third stage was collected directly on a Buchner funnel, and the feed was replenished periodically to maintain operation for 12 h.

2.3. General Procedure for Ultrasound Experiments. All experiments were performed in a 1 L cylindrical jacketed vessel equipped with an overhead stirrer, glass retreat curve

https://doi.org/10.1021/acs.oprd.1c00209
Org. Process Res. Dev. 2021, 25, 2119−2132

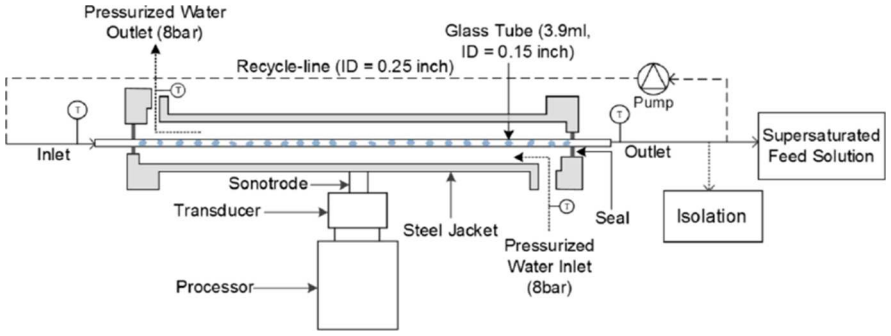

Figure 4. P&ID of the ultrasound flow cell.

impeller (three-blade, 68 mm diameter), temperature probe, condenser, and Mettler-Toledo G-400 FBRM probe (Figures 4 and 5). The ultrasound flow cell (GDmini2, Hielscher, Telt

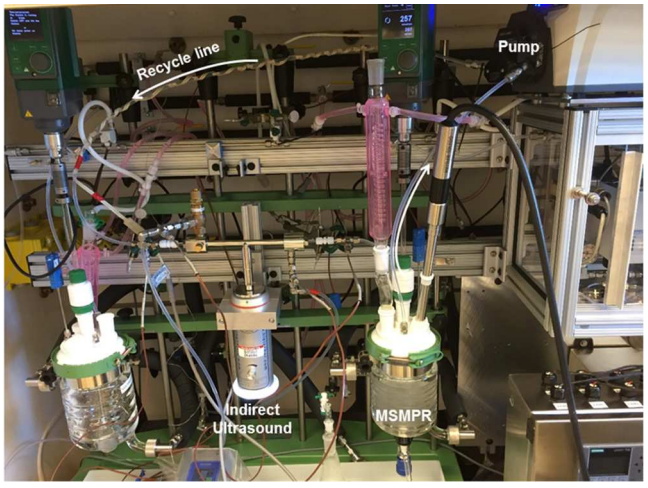

Figure 5. Ultrasound experimental setup.

Germany) was equipped with a glass tube (3.9 mL, ID: 0.15 inch) and connected to the crystallizer using 1/4″ polytetrafluoroethylene (PTFE) tubing (Figure 4). J-type thermocouples were installed on the flow-cell inlet and outlet for temperature monitoring. The flow cell was coupled with a UP200St-TD transducer (200 W), and pressurized water (8 bar) was used to control its temperature and transfer the ultrasonic vibrations to the glass tube. The ultrasound was operated continuously at a frequency of 26 kHz, and power amplitudes of 20, 40, and 80% were investigated.

A Masterfex peristaltic pump (Masterflex L/S equipped with pump head 77390-00) was installed between the flow cell and the 1 L reactor (Figure 5). Stirring was initiated at 250 rpm, and the API (70 g) was dissolved in a 70/30 v/v % MeOH/H_2O (1 L, 14.3 vol) mixture at 70 °C. Once there were no solids remaining, as indicated by the G-400 FBRM probe, the temperature was adjusted to 45 °C, to generate a supersaturated solution (s = 1.61), and the Masterflex pump followed by the ultrasound transducer was initiated at the desired settings.

2.4. Laser Diffraction Particle Size Method. A Malvern Mastersizer 2000 instrument equipped with a wet dispersion unit and Hydro Sight was used for all laser diffraction particle size analyses. Standard instrument settings were as follows: Mie evaluation mode, a product refractive index setting of 1.52, a dispersant refractive index of 1.38, a dispersion unit speed of 1500 rpm, a saturated solution of API in 2-propanol was used as the dispersant, a sample measurement time of 10 s, a 5−15% obscuration limit, and 30% sonication were used. A total of three measurement cycles were performed, and the average value was reported.

Approximately, 10 mL of the slurry was removed from the crystallizer using a transfer pipette whose tip was cut. The solid sample was isolated by filtration and dried in a vacuum oven at 45 °C for overnight before the measurement. The dry powder was dispersed in saturated 2-propanol and added dropwise to the wet dispersion unit to give the desired obscuration, typically around 7%.

2.5. HPLC Method. The high-performance liquid chromatography (HPLC) method used for concentration measurement and for analyzing the purity of the final product employed a symmetry C 18.5 μm 4.5 × 75 mm column, maintained at 25 °C, and was run on an Agilent 1100 Series. A 0.1% formic acid in H_2O solution was used as mobile phase A, and a 0.1% formic acid in CH_3CN solution was used as mobile phase B. The total flow rate was set to 1.0 mL/min, the injection volume was 5.0 μL, and the detection was carried out at 230 nm. The total method analysis time was 10 min. A gradient was used starting at 90% of mobile phase A, moving to 60% after 5 min, and ending back up at 90% at 6 min. The latter composition was maintained for 1 min after which time the eluent was switched to 100% mobile phase B for 4 min. Finally, the column was re-equilibrated at 100% mobile phase A for a total of 4 min.

The sample preparation procedure was as follows: (1) for concentration analysis, approximately 1 mL of the slurry was removed from the crystallizer using a syringe and filtered through a 0.2 μm syringe filter into a preweighed 50 mL volumetric flask. The resultant mother liquor was diluted with a CH_3CN/H_2O (50/50 v/v %) mixture to 50 mL; (2) for purity analysis, 25 mg of API was dissolved in a 25 mL volumetric flask using 70/30 v/v % MeOH/H_2O. API was eluted at approximately 4.2 min.

2.6. Sampling Protocol. Regular sampling was implemented throughout the duration of each experiment. For concentration analysis, slurry samples (5 mL) were directly withdrawn from the vessel and immediately filtered *via* a syringe filter (0.2 μm) into a preweighed volumetric flask (25 mL). The relevant diluents for HPLC measurement were then used (Section 2.5). For each sampling time, triplicates were taken for a consistency check. For particle size distribution analysis, 25−50 mL (depending on slurry density) was directly withdrawn from the vessel using a transfer pipette and immediately filtered *via* vacuum filtration, washed with the same solvent composition used for the crystallization, and

https://doi.org/10.1021/acs.oprd.1c00209
Org. Process Res. Dev. 2021, 25, 2119−2132

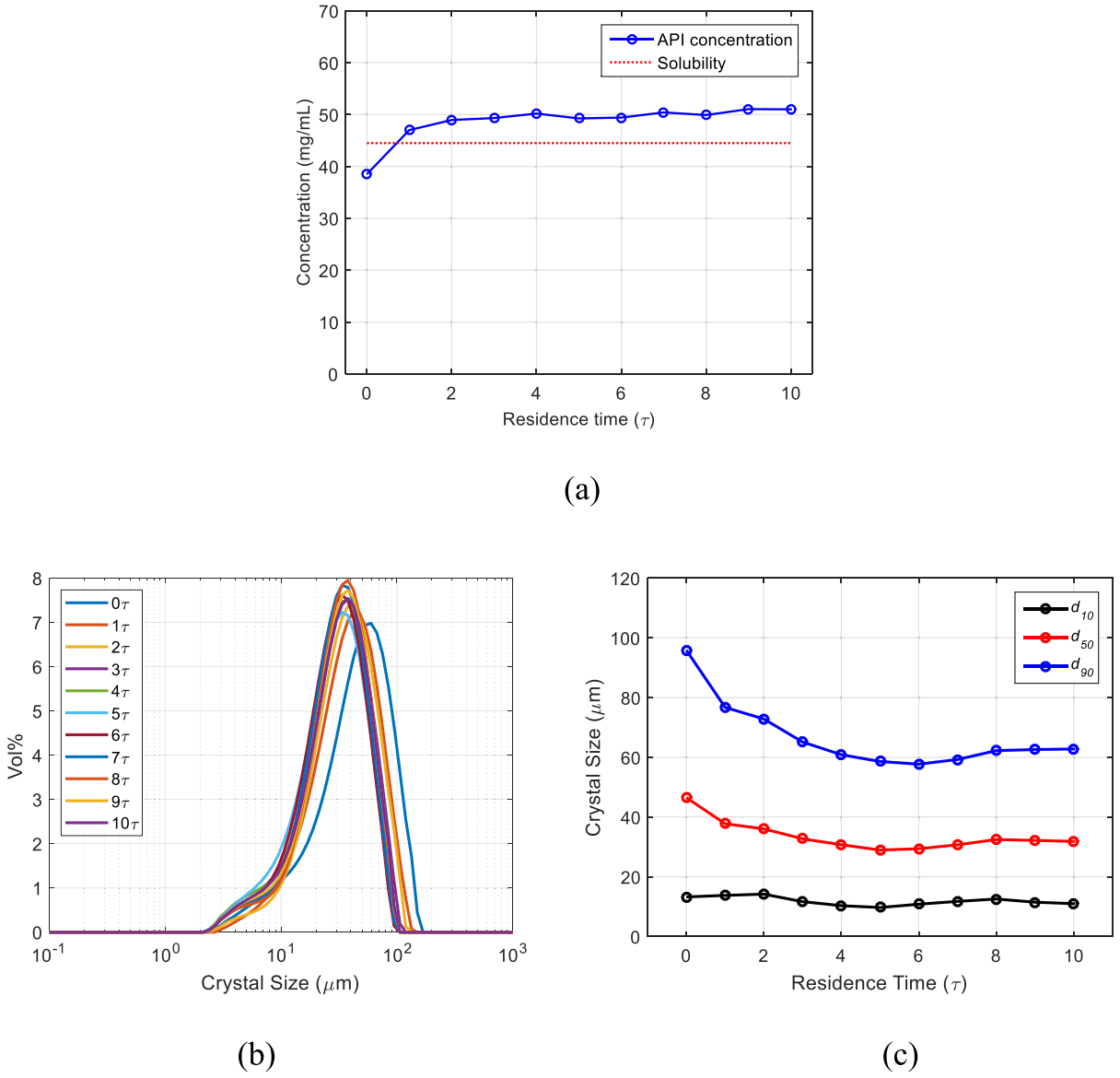

Figure 6. a) Concentration and (b) PSD results as a function of residence time for a one-stage continuous crystallization experiment operated at 45 °C with a 30 min residence time and an external wet mill set at 10,000 rpm with a TOPRT of 15.

dried in a vacuum oven overnight (40−45 °C). Dried samples were then further subjected for microscopic and particle size analysis.

3. RESULTS AND DISCUSSION

3.1. Use of Wet Milling to Control Nucleation. In order to address the issues observed with the poor nucleation kinetics of API, resulting in washout and extreme fouling, wet milling was investigated both as part of an external recirculation loop and directly installed within the first stage of a cascade of continuous stirred reactors. A proof-of-concept single-stage crystallization using the former configuration and an IKA MagicLab wet mill was successfully conducted and operated for a total of 10 residence times (τ) without any fouling. An undersaturated solution of API (70 mg/mL) in 70/30 v/v % MeOH/H_2O at 65 °C was fed to the crystallizer that was operated at 45 °C with the wet mill running at 10,000 rpm. At this temperature, if the system fully desupersaturated, approximately 36% of the product was expected to crystallize, as the solubility of API at 45 °C is 44.5 mg/mL. This is typical in the design of a three-stage MSMPR process, where the amount of material deposited in each stage is divided equally across the total number of reactors used. The residence time was set to 30 min, while the turnover number per residence (TOPRT) time, which is defined as the number of times the slurry is recycled through the wet mill during one residence time, was 15. The TOPRT can be calculated from the recycle volumetric flow rate through the wet mill and the volumetric flow rate through the MSMPR using the following equation

$$\mathrm{TOPRT} = \frac{q_{\mathrm{mill}}\tau}{V} \tag{1}$$

where V is the MSMPR operating volume, τ is the MSMPR residence time, and q_{mill} is the recycle volumetric flow rate through the wet mill.

The system startup was achieved by charging 35 g of API to the crystallizer followed by 0.6 L of a 70/30 v/v % MeOH/H_2O mixture. The jacket temperature of the crystallizer was set to 45 °C. The wet mill was then initiated and operated at the

https://doi.org/10.1021/acs.oprd.1c00209
Org. Process Res. Dev. 2021, 25, 2119−2132

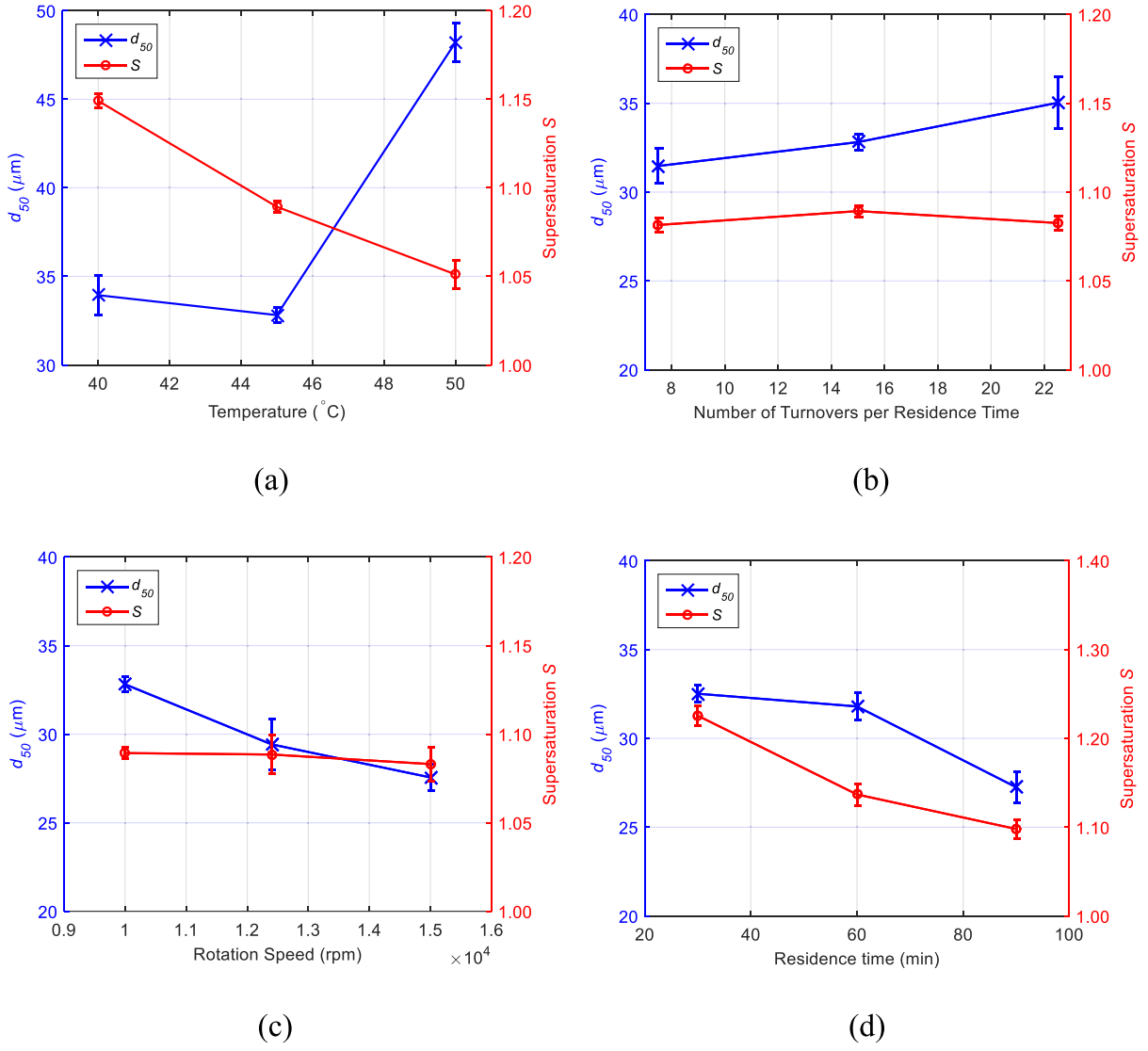

Figure 7. Optimization of the single-stage MSMPR equipped with the IKA magicLAB wet mill: (a) impact of the crystallizer T on steady-state concentration and PSD (wet mill rpm = 10,000, τ = 30 min, and TOPRT = 15); (b) impact of TOPRT on steady-state concentration and PSD (wet mill rpm = 10,000, τ = 30 min, and T = 45 °C); (c) impact of wet mill rotational speed on steady-state concentration and PSD (τ = 30 min, TOPRT = 15, and T = 45 °C); and (d) impact of the crystallizer τ on steady-state concentration and PSD (wet mill rpm = 12,400 and T = 45 °C).

desired setting until the PSD of the suspension was equilibrated, typically 30 min, after which time the feed pump was switched on. At 10,000 rpm and using the wet mill configured with the three fine rotors, the d_{50} of the product at the end of the equilibration period was 45 μm. This defined the smallest PSD that could be obtained through crystal breakage. As can be seen from Figure 6, the crystallizer's concentration rapidly reached the steady state (within 2τ) and was operated at a relatively low supersaturation of 1.12. It is worth mentioning that at τ = 0, the concentration was below the compound's solubility at 45 °C. This is because the temperature in the crystallizer was lower than 45 °C due to the cooling jacket of the wet mill. Once the hot feed started to pump in, the temperature in the crystallizer was well controlled to 45 °C. The particle size distribution took a total of 4τ to reach the steady state and stabilized at a d_{50} of 32 μm, approximately 20% smaller than the initial PSD, presumably as a result of shear-induced secondary nucleation. The slight upward inflection in d_{50} and d_{90} above 6τ is within the measurement error. Therefore, all subsequent experiments were run for a total of 8τ to ensure the steady state. It was found that the use of the FBRM and UV or mid FT-IR to monitor in real time chord length distributions and concentration, respectively, during the continuous experiments was unreliable due to fouling of the probes. As a result, samples were removed every 2τ for offline concentration and PSD analysis to confirm the steady state.

Four parameters were investigated in an attempt to minimize the product particle size and the supersaturation within the crystallizer in order to control encrustation: reactor temperature (T), TOPRT, milling speed, and τ (Figure 7). The optimization was conducted in a one-variable-at-a-time (OVAT) study and started with the investigation of the impact of the crystallizer temperature and therefore crystallization driving force. The milling speed, TOPRT, and residence time of the MSMPR were set at 10,000 rpm, 15, and 30 min, respectively, and a total of three temperatures were investigated, 50, 45, and 40 °C. These corresponded to equilibrium concentrations of 56.0, 44.5, and 35.2 mg/mL, respectively, that would result in 20, 36, and 50%, respectively,

https://doi.org/10.1021/acs.oprd.1c00209
Org. Process Res. Dev. 2021, 25, 2119−2132

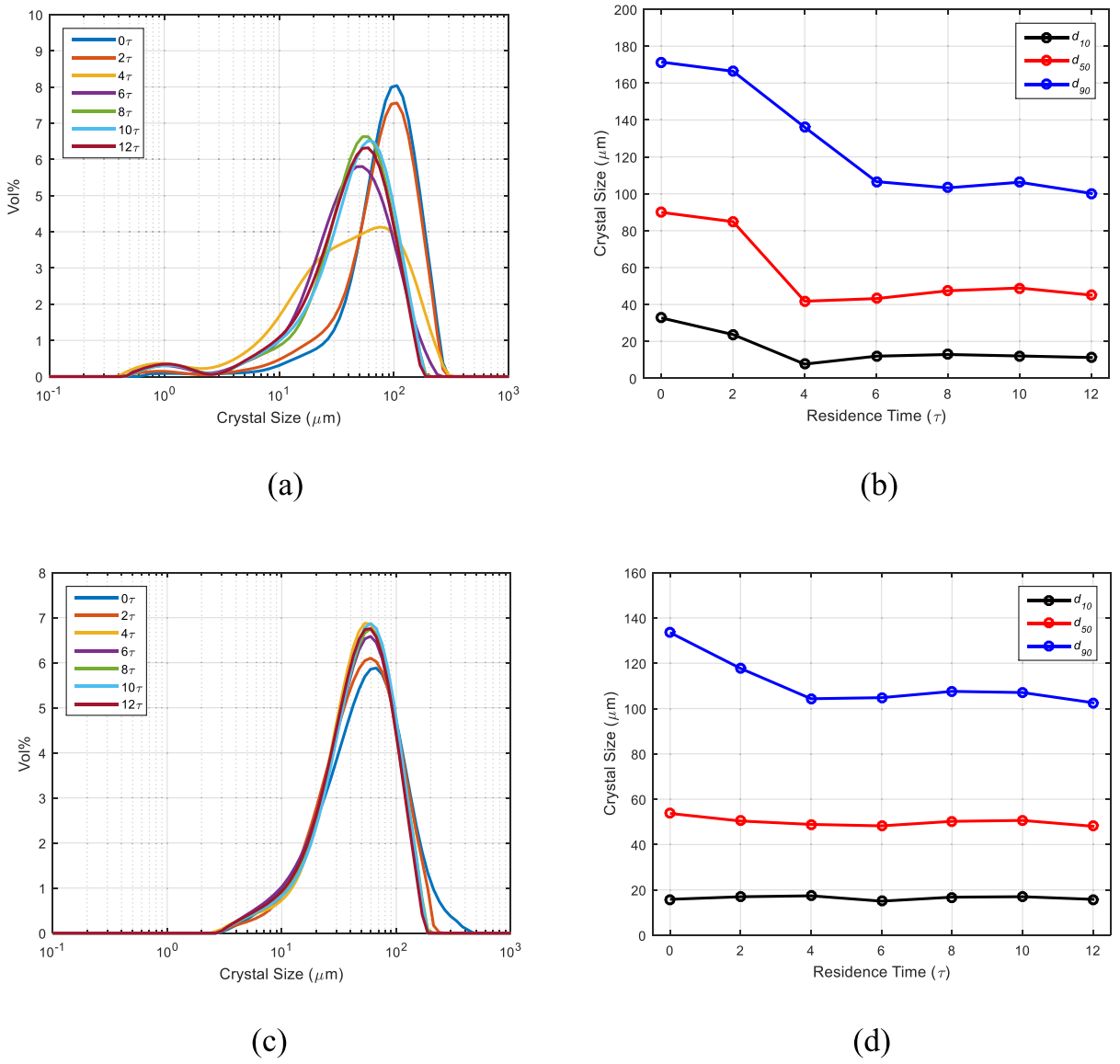

Figure 8. Comparison of startup modes for a one-stage continuous crystallization experiment operated at 45 °C with a 90 min residence time and an immersion mill set at 10,000 rpm: (a,b) PSD as a function of τ for a startup from a saturated suspension and (c,d) PSD as a function of τ for a startup from a batch crystallization.

of the product being crystallized assuming full desupersaturation. The results from these experiments are outlined in Figure 7a. As expected, the steady-state supersaturation increased from 1.05 to 1.15 as the T decreased from 50 to 40 °C, and more solute is available for crystal growth and/or nucleation. The particle size at the steady state, as indicated by the d_{50}, dropped significantly from 48 to 32 μm as the temperature was reduced from 50 to 45 °C. This is most likely a result of the higher supersaturation at 45 °C, resulting in more secondary nucleation during the crystallization. Interestingly, no significant change in steady state d_{50} was observed when the temperature decreased from 45 to 40 °C, which is probably because the reduction on particle size reached the limit of the wet mill. As our objective was to generate the smallest possible particle size material while balancing steady-state supersaturation in order to mitigate encrustation, an operating T of 45 °C was selected.

TOPRT was varied from 7.5 to 22.5 to investigate its impact on steady-state PSD and supersaturation. When the MSMPR τ was set to 30 min, this TOPRT range corresponded to adjusting the flow rate through the wet mill from 150 to 400 mL/min. The milling speed and crystallizer T were fixed at 10,000 rpm and 45 °C, respectively, and the results of this study are shown in Figure 7b. It was found that a slightly smaller PSD was obtained at the lower TOPRT (d_{50} of 31 *vs* 35 μm for a TOPRT of 7.5 *vs* 22.5) that could be a result of the longer residence time within the wet mill, resulting in increased breakage and/or secondary nucleation. Based on these data, it would also appear that the τ in the mill had a larger effect on particle size than the overall turn-over number of the crystallizer. Nevertheless, over the investigated range, the TOPRT had a negligible impact on both the steady-state PSD and supersaturation. This suggests that the values for TOPRT used in our experiment were in the attrition regime, where particles have already been reduced by chipping and further milling results in no significant size reduction.[49,50]

Next, the impact of the wet mill rotational speed was investigated focusing on higher speeds in an attempt to obtain

https://doi.org/10.1021/acs.oprd.1c00209
Org. Process Res. Dev. 2021, 25, 2119−2132

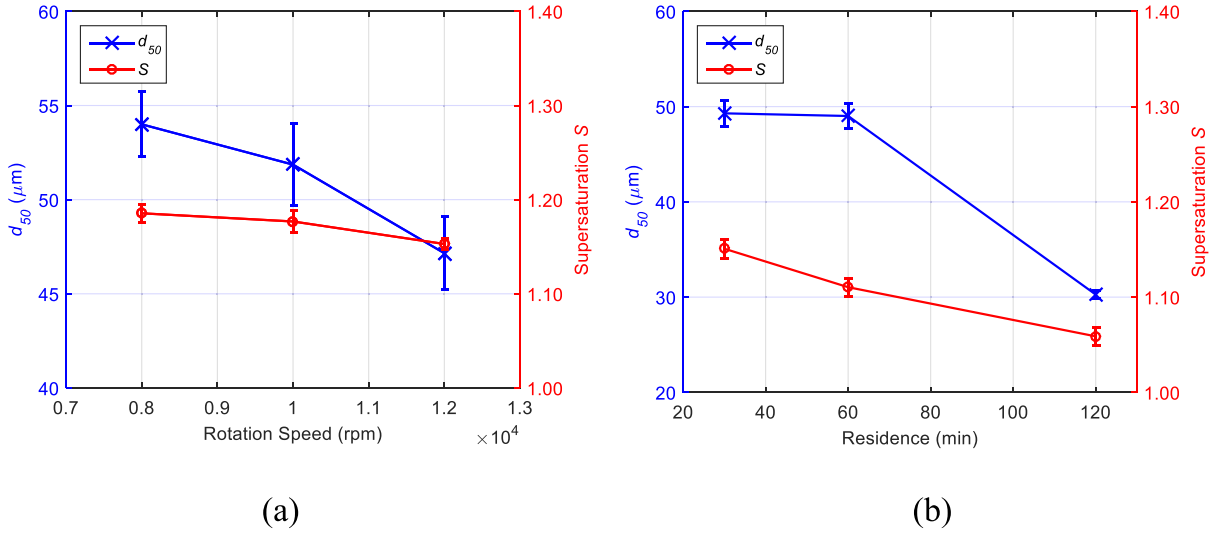

Figure 9. Optimization of the single-stage MSMPR equipped with an immersion mill: (a) impact of mill rotational speed on steady-state concentration and PSD (τ = 30 min and T = 45 °C) and (b) impact of the crystallizer τ on steady-state concentration and PSD (mill rpm = 12,000 and T = 45 °C).

smaller PSD materials and further reduce steady-state supersaturation through increased secondary nucleation. While the wet mill is capable of operating at a maximum speed of 26,000 rpm, control of the crystallizer temperature became increasingly challenging beyond 15,000 rpm, requiring a significant temperature drop across the vessel jacket. Therefore, the maximum rotational speed was restricted to 15,000 rpm. The TOPRT, crystallizer T, and τ were 15, 45 °C and 30 min, respectively. As can be seen from Figure 7c, milling speed only affected the particle size of the product, affording a d_{50} of 27.6 μm when 15,000 rpm was used *versus* 32.8 μm at 10,000 rpm. However, temperature control became challenging even at a milling speed of 15,000 rpm. The jacket temperature of the wet mill needs to be set lower than 5 °C, which could result in fouling and blockage over extended run times. Therefore, 12,400 rpm was selected as the optimal speed.

Finally, the effect of τ of the MSMPR was studied, with the maximum time limited to 90 min, primarily driven by a desire to maintain a reasonable productivity for the process. Since the TOPRT is dependent on τ, fixing it would require adjusting, for each experiment, the flow rate of the recirculation loop through the mill. As it was earlier demonstrated that TOPRT had a small impact on PSD across the range investigated (<10%), the pump before the wet mill that restricted flow through the mill was removed, so that the recirculation rate was determined by the mill rotational speed, which was around 900 mL/min when 12,400 rpm was used. This corresponded to a TOPRT range of 45−135 across the τ investigated. Furthermore, in earlier experiments, some fouling of the return loop from the wet mill to the MSMPR was observed that could result in blockage upon prolonged operation. Therefore, that section of the recirculation loop was heated 5 °C above the crystallizer temperature, that is, to 50 °C. The experimental results are shown in Figure 7d, and as expected, they show that steady-state supersaturation decreases with increasing τ as the system is given more time to desupersaturate. Interestingly, the supersaturation is overall much higher in this set of experiments (*e.g.*, when τ = 30 min and s = 1.23 *vs* 1.12 without the heated return loop), which could be attributed to dissolution of the generated fines, as a result of the heated return loop. For this set of experiments, the τ through the wet mill was constant and an overall longer crystallizer τ effectively resulted in a higher turn-over number and therefore a lower particle size (27.3 μm when τ = 90 min).

However, there was a concern about the robustness of the external wet mill over prolonged operation during manufacturing particularly with regard to potential leaks as seals degraded, managing the temperature drop across the recirculation loop and the numerous surfaces available for nucleation that could lead to encrustation and ultimately blockage. Therefore, the use of an immersion mill was evaluated that was placed directly within the crystallizer and replaced the overhead agitator. The mill was used both to agitate the reactor contents and to control nucleation and particle size.

Startup from a batch crystallization was found to be more effective than from a saturated suspension, affording a tighter PSD and allowing the system to reach the steady state within 4 *versus* 6 τ (Figure 8). Accordingly, 35 g of API was charged to the crystallizer followed by 0.5 L of a 70/30 v/v % MeOH/H_2O mixture. The mill was switched on to the desired setting (10,000 rpm), and the resulting slurry was heated to 60 °C until all solids were fully dissolved. The solution was then cooled to 45 °C, at which point an undersaturated solution of API (70 mg/mL) in 70/30 v/v % MeOH/H_2O at 65 °C was fed to the crystallizer at 16.67 mL/min, corresponding to a τ of 30 min. This afforded a steady-state d_{50} of 52 μm and a supersaturation of 1.18. The mill rotational speed and crystallizer τ were then optimized through a series of OVAT studies (Figure 9). The range of speeds investigated was 8000−12,000 rpm, as at lower speeds, solids were not fully suspended and at higher ones, control of the reactor temperature became extremely challenging. As expected, the higher the mill speed, the lower the steady state particle size (54 *vs* 47 μm at 10,000 *vs* 12,000 rpm). The impact on the supersaturation was minimal and varied from 1.19 to 1.15 (Figure 8a). A slightly wider residence time range than that investigated with the external wet mill was explored (30−120 min) and found to have the largest impact on both the steady-state supersaturation and particle size. These ranged between 1.15 and 1.06 and 49−30 μm, respectively, with higher τ

https://doi.org/10.1021/acs.oprd.1c00209
Org. Process Res. Dev. 2021, 25, 2119−2132

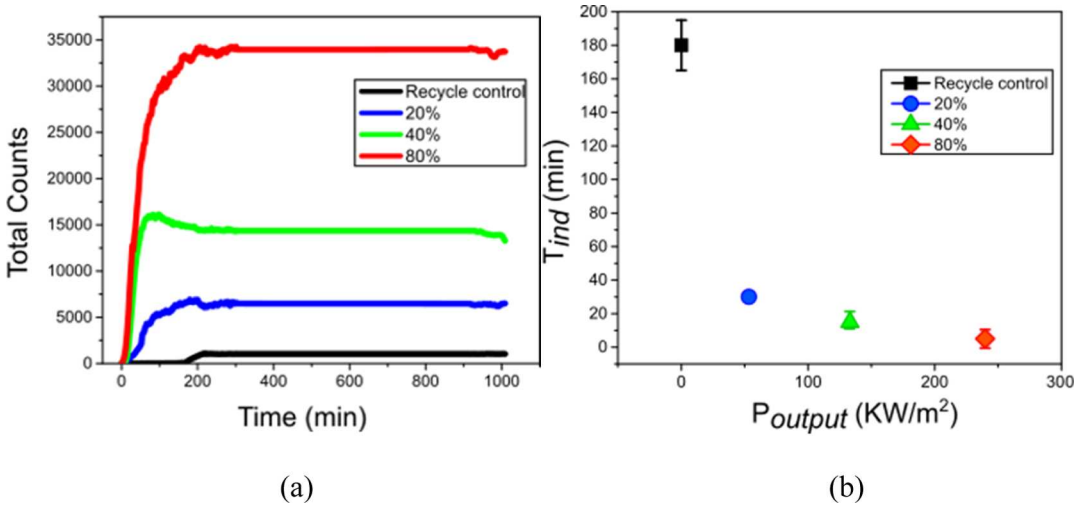

Figure 10. Evolution of total count profiles (a) and induction time for API (b) as a function of ultrasound power.

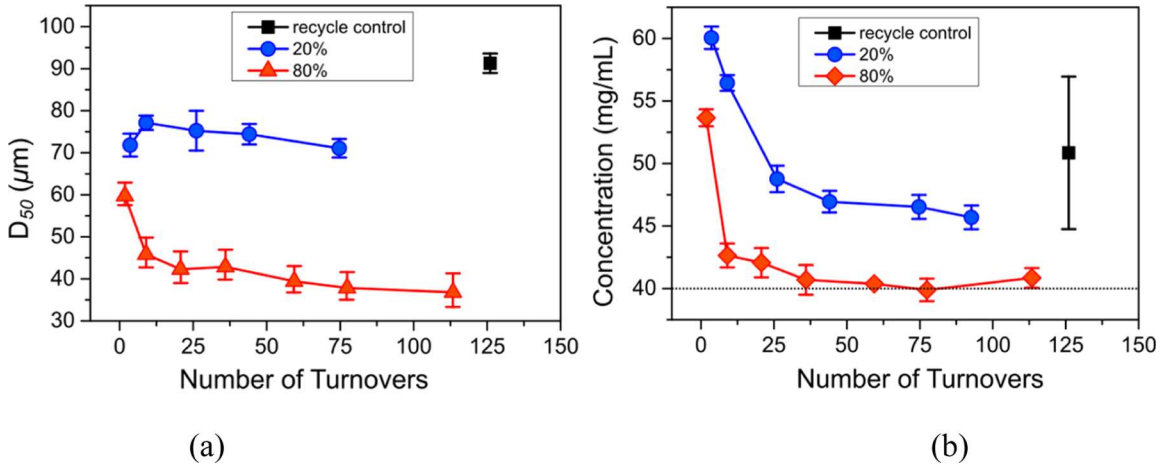

Figure 11. Impact of ultrasound amplitude on particle size (a) and desupersaturation rate (b) over the course of isothermal API crystallization experiments using an external ultrasound flow cell.

affording smaller particle sizes and lower supersaturations as the system is given more time to desupersaturate and the mill TOPRT is higher. Overall, it was found that both mills were capable of maintaining similar levels of supersaturation within the crystallizers and afforded similar particle sizes. Most importantly, both systems were able to maintain the steady state and minimize encrustation by effectively controlling nucleation. However, it did not prove possible to generate particle sizes of <30 μm under these conditions.

3.2. Use of Sonication to Control Nucleation. Sonication was next investigated as a means of controlling nucleation and potentially generating a smaller particle size material than could be obtained through a mechanical mill. A flow cell (GDmini2, Hielscher, Germany) was used consisting of a resonating stainless-steel jacket around a glass tube that was connected to the crystallizer using PTFE tubing (Figure 4). The flow cell was coupled with a UP200St-TD transducer (200 W), and temperature-controlled pressurized water was used as a coolant and to transfer the ultrasonic vibrations to the glass tube and therefore sonicate the liquid flowing through the tube. This resulted in a more uniform transfer of power across the process stream. The coolant also allowed for accurate control of the process temperature, enabling the continuous operation of the transducer, in contrast to immersion probes that can often only be used intermittently to avoid uncontrolled heating. Furthermore, in this configuration, the probe did not come into direct contact with the process stream, avoiding any potential contamination from degradation of the probe. It was also anticipated that this setup could afford a much more robust solution for controlling nucleation, as it was unobstructed with no moving parts and the ultrasound could prevent encrustation within the nucleation device.

The effectiveness of this device as a nucleator at different amplitudes was evaluated by measuring induction times. The flow cell was installed on a recirculation loop attached to a 1 L crystallizer equipped with an FBRM probe. A supersaturated solution (s = 1.61) of API in 70/30 v/v % MeOH/H_2O at 45 °C was recirculated at 300 mL/min in the absence of ultrasound for 0.5−1 h to allow for the temperature to stabilize and to confirm the absence of primary nucleation. After this initial period, the desired ultrasound power amplitude was selected and applied in the continuous mode throughout the duration of each experiment.

Indirect sonication had a considerable impact on induction time (Figure 10). Increasing the power amplitude from 0 to 80% (239.97 kW/m^2) reduced the mean induction time from 180 to 5 ± 5.51 min (Figure 10b). Selecting the highest power

https://doi.org/10.1021/acs.oprd.1c00209
Org. Process Res. Dev. 2021, 25, 2119−2132

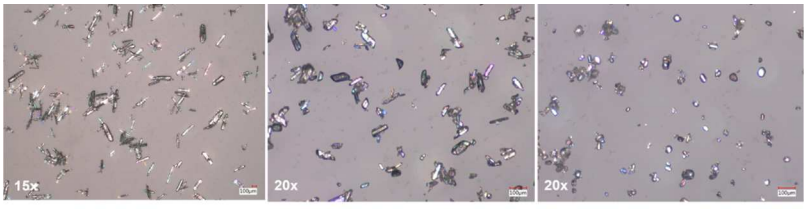

Figure 12. Impact of ultrasound amplitude for the following conditions: (a) recycle control, (b) 20, and (c) 80% over the course of isothermal API crystallization experiments using an external ultrasound flow cell.

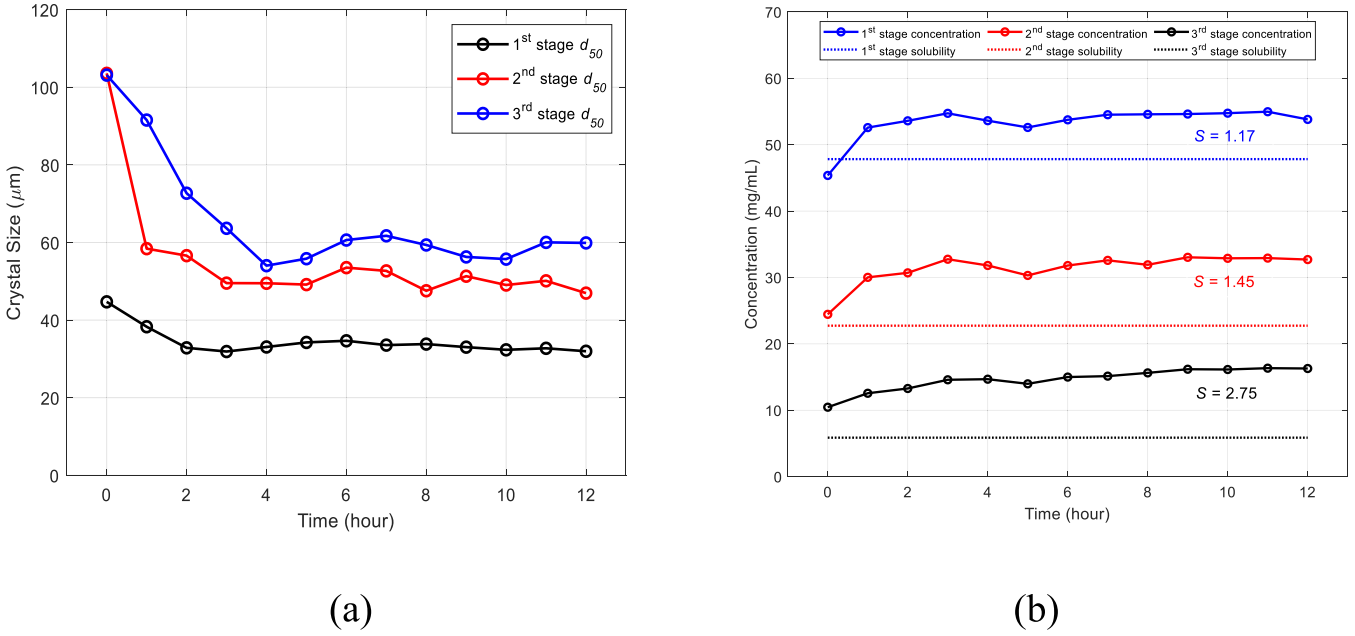

Figure 13. Time course particle size (a) and concentration data (b) of each of the three stages for the continuous 12 h MSMPR crystallization experiment.

amplitude of 80% (239.97 kW/m^2) produced an instantaneous occurrence of nucleation within 5 min of ultrasound start (Figure 10b). This generated a rapid increase in total counts from 0 to 50 min due to enhanced secondary nucleation which leveled off after 200 min as the supersaturation is depleted (Figure 10a).

The initial strategy was to operate in a continuous single-pass mode without recirculation by feeding an undersaturated solution (70 mg/mL) through the ultrasound flow cell at different temperatures and hence supersaturations (35, 40, and 45 °C corresponding to supersaturation values of 2.6, 2, and 1.6, respectively). This would allow for the flow cell to be positioned between the feed tank and the first stage of a multistage MSMPR crystallizer effectively separating nucleation from growth. Based on the induction time measurements, the transducer would need to be operated at the maximum amplitude. Initial testing was successful in inducing nucleation with short τs (11−55 s), but there were significant challenges with the onset of fouling in the transfer lines as a result of the extremely low flow rates required to achieve the target τ values (4−20 mL/min). Furthermore, as a result of the API's fast growth kinetics, significant growth was observed, producing large particles that as a result of the low flow velocities sedimented in the lines leading to blockage. This approach was therefore not feasible and efforts were directed toward incorporating the flow cell in a recirculation loop, in a similar configuration to that used with the external wet mill.

Isothermal batch experiments were conducted during which a 70 mg/mL solution of API was prepared in 70/30 v/v % MeOH/H_2O at 60 °C, which was then cooled to 45 °C to generate a supersaturated solution (s = 1.61). This solution was recirculated through the flow cell at 300 mL/min investigating different ultrasound amplitudes (0, 20, and 80%). The particle size and desupersaturation data for these experiments are shown in Figure 11. A significant particle size reduction was achieved when an 80% amplitude was used, affording a d_{50} of 36.80 μm *versus* 71.07 and 91.28 μm when 20% or no ultrasound was applied, respectively. Deagglomeration of the particles was observed, and the elongated rod-shaped particles became more circular (Figure 12a−c). The concentration profiles obtained for the 20 and 80% ultrasound conditions show a rapid decline within 25 turnovers, after which a slow decrease from 25 to 125 turnovers is observed (Figure 11b). For 80%, overall depletion of concentration was considerably quicker than 20% which approached the solubility limit at 40 mg/mL, indicating complete desupersaturation. This was expected as 80% had a shorter mean induction time than 20% and therefore faster nucleation kinetics. As the experiments were conducted under isothermal conditions, supersaturation consumption is preceded by the rapid nucleation burst at 80% due to the creation of a large available

https://doi.org/10.1021/acs.oprd.1c00209
Org. Process Res. Dev. 2021, 25, 2119−2132

crystal surface area for subsequent growth and supersaturation depletion.

While promising results from using the sonication method were observed, the particle size limit achieved was 36.80 μm. This was comparable with the single-stage MSMPR wet milling experiments which had reached sizes of ~30 μm. Although targeting smaller size ranges of 2−11 μm proved challenging, both techniques demonstrated the capability to reduce the nucleation onset for API and the potential to be deployed as nucleator devices. However, when compared to the application of high-shear rotor-stator devices in pharmaceutical manufacturing, the indirect sonication approach remains at low technology readiness levels. Further work is therefore required to better understand the fundamental performance of the system as a controllable, robust external field generator and address operational challenges such as scale-up, continuous running, and performance with different compounds. Therefore, the development of the continuous MSMPR crystallizer proceeded with wet milling incorporated within the first stage.

3.3. Development of a Three-Stage MSMPR Crystallization Process. A continuous crystallization experiment was performed in order to assess the robustness of using the external wet mill to control nucleation. A three-stage configuration was selected to provide the system with enough residence time and temperature drop (from 60 to 5 °C), required to maintain a reasonable productivity, while maintaining low steady-state supersaturations to manage fouling. The optimal operating parameters for stage 1 were determined through the OVAT experiments described earlier in the manuscript and consisted of a process temperature of 45 °C and a wet mill rotational speed of 12,400 rpm. The temperature of the second stage was set at 30 °C, while that of the third stage was set at 5 °C. All three stages operated at a τ of 30 min, resulting in a total system τ of 90 min. The system was initiated from suspensions, and the process was successfully operated for more than 12 h without blockages (corresponding to eight residence times). The PSD and concentration evolution in each stage are presented in Figure 13. The PSD of the first stage reached the steady state in 2 h, while that of the second and third stages achieved the steady state after 3 and 4 h (Figure 13a), respectively. The steady state d_{50} was 32, 49, and 60 μm for the first, second, and third stage, respectively. The concentration in each stage stabilized in less than 3 h. The steady-state concentration in each stage was 54.8, 32.9, and 16.2 mg/mL, respectively, which corresponded to supersaturation values of 1.14, 1.45, and 2.75 (Figure 13b). The yield of this continuous run was 77% w/w. The second and third stage, in particular, operated at relatively high supersaturation, indicating that longer residence times would be required to improve efficiency. Some fouling in the transfer lines was observed that necessitated them being manually cleaned every two residence times (3 h) to avoid blockage. This was achieved by alternating between two sets of lines that were cleaned in between use. Post transfer, it was impossible to blow the lines dry and any residual liquid gradually nucleated as the lines were not heated. Heated transfer lines are critical for maintaining control in this context, and an automated way of cleaning the lines would be beneficial. The flow rate through the wet mill gradually dropped from about 900 to 645 mL/min, indicating some degree of fouling. This indicated that in order to run for longer durations, two wet mills may be required configured with external cleaning loops and a feedback control system to trigger a cleaning cycle when flow rates drop below a certain level. Finally, even though the fouling on the reactor walls was minimal during the 12 h run, a control strategy for its management is required. It can be envisioned that oscillating the jacket temperature would result in brief elevated reactor wall temperatures that may be sufficient to dissolve any nuclei that may have deposited on them and ultimately manage fouling.[51]

4. CONCLUSIONS

A particle engineering strategy for providing control over the final particle size distribution and overcoming the challenges to fouling and encrustation during continuous crystallization development has been investigated for the API.

The API was prone to slow nucleation behavior while exhibiting fast growth kinetics. By introducing high shear wet milling and indirect sonication through similar intensified strategies, both techniques were found to rapidly initiate the onset and provide good control over nucleation and fouling. This was experimentally evaluated through the effect of a number of key processing parameters (supersaturation, temperature, mill rotational speed, ultrasound power output, and number of turnovers) on product attributes (size and size distribution), where the target was to generate small sizes for seeding purposes. This proved challenging as the size limit achieved from both strategies ranged from 28 to 37 μm. However, and equally importantly, well-controlled seeds were generated without the need for an offline milling step and fouling was mitigated allowing for the development of a continuous MSMPR process. The high shear wet mill was pursued over sonication as the *in situ* seeding route and this technology were demonstrated in running a three-stage MSMPR crystallization process. Finally, areas of improvement to the overall process design were identified that if optimized would allow for robust operation over a prolonged duration suitable for pharmaceutical manufacturing applications.

AUTHOR INFORMATION

Corresponding Authors

Yihui Yang − *Process Chemistry and Development, Takeda Pharmaceuticals International Company, Cambridge, Massachusetts 02139, United States;* orcid.org/0000-0002-0485-7680; Email: yihui.yang@takeda.com

Alastair J. Florence − *EPSRC Future CMAC Manufacturing Research Hub, Institute of Pharmacy & Biomedical Sciences, Technology and Innovation Centre, University of Strathclyde, Glasgow G1 1RD, U.K.;* orcid.org/0000-0002-9706-8364; Email: alastair.florence@strath.ac.uk

Authors

Bilal Ahmed − *EPSRC Future CMAC Manufacturing Research Hub, Institute of Pharmacy & Biomedical Sciences, Technology and Innovation Centre, University of Strathclyde, Glasgow G1 1RD, U.K.; EPSRC Future CMAC Manufacturing Research Hub, Department of Chemical and Biological Engineering, University of Sheffield, Sheffield S1 3JD, U.K.*

Christopher Mitchell − *Process Chemistry and Development, Takeda Pharmaceuticals International Company, Cambridge, Massachusetts 02139, United States*

Justin L. Quon − *Process Chemistry and Development, Takeda Pharmaceuticals International Company, Cambridge, Massachusetts 02139, United States*

https://doi.org/10.1021/acs.oprd.1c00209
Org. Process Res. Dev. 2021, 25, 2119−2132

Humera Siddique − *EPSRC Future CMAC Manufacturing Research Hub, Institute of Pharmacy & Biomedical Sciences, Technology and Innovation Centre, University of Strathclyde, Glasgow G1 1RD, U.K.*

Ian Houson − *EPSRC Future CMAC Manufacturing Research Hub, Institute of Pharmacy & Biomedical Sciences, Technology and Innovation Centre, University of Strathclyde, Glasgow G1 1RD, U.K.*

Charles D. Papageorgiou − *Process Chemistry and Development, Takeda Pharmaceuticals International Company, Cambridge, Massachusetts 02139, United States;* orcid.org/0000-0001-7959-6289

Complete contact information is available at: https://pubs.acs.org/10.1021/acs.oprd.1c00209

Notes

The authors declare no competing financial interest.

■ ACKNOWLEDGMENTS

B.A., I.H., H.S., and A.J.F. would like to thank EPSRC and the Doctoral Training Centre in Continuous Manufacturing and Crystallisation (grant ref: EP/K503289/1) and the EPSRC Future Continuous Manufacturing and Advanced Crystallisation Research Hub (CMAC, grant ref: EP/P006965/1) for partially funding the investigation of the use of sonication to control nucleation. All other research was conducted by Takeda employees and funded by the company. Data underpinning the sonication section of this publication is openly available from the University of Strathclyde Knowledgebase at https://doi.org/10.15129/d31b0703-470b-4ad3-9037-d797e017887b.

■ REFERENCES

(1) Leane, M.; Pitt, K.; Reynolds, G. K.; Dawson, N.; Ziegler, I.; Szepes, A.; Crean, A. M.; Dall Agnol, R.; The Manufacturing Classification System (MCS) Working Group. Manufacturing classification system in the real world: factors influencing manufacturing process choices for filed commercial oral solid dosage formulations, case studies from industry and considerations for continuous processing. *Pharm. Dev. Technol.* **2018**, *23*, 964−977.

(2) Variankaval, N.; Cote, A. S.; Doherty, M. F. From form to function: Crystallization of active pharmaceutical ingredients. *AIChE J.* **2008**, *54*, 1682−1688.

(3) Mascia, S.; Heider, P. L.; Zhang, H.; Lakerveld, R.; Benyahia, B.; Barton, P. I.; Braatz, R. D.; Cooney, C. L.; Evans, J. M. B.; Jamison, T. F. End-to-end continuous manufacturing of pharmaceuticals: integrated synthesis, purification, and final dosage formation. *Angew. Chem., Int. Ed.* **2013**, *52*, 12359−12363.

(4) Nasr, M. M.; Krumme, M.; Matsuda, Y.; Trout, B. L.; Badman, C.; Mascia, S.; Cooney, C. L.; Jensen, K. D.; Florence, A.; Johnston, C. Regulatory perspectives on continuous pharmaceutical manufacturing: moving from theory to practice: September 26-27, 2016, international symposium on the continuous manufacturing of pharmaceuticals. *J. Pharm. Sci.* **2017**, *106*, 3199−3206.

(5) Cole, K. P.; Reizman, B. J.; Hess, M.; Groh, J. M.; Laurila, M. E.; Cope, R. F.; Campbell, B. M.; Forst, M. B.; Burt, J. L.; Maloney, T. D. Small-volume continuous manufacturing of merestinib. Part 1. Process development and demonstration. *Org. Process Res. Dev.* **2019**, *23*, 858−869.

(6) Reizman, B. J.; Cole, K. P.; Hess, M.; Burt, J. L.; Maloney, T. D.; Johnson, M. D.; Laurila, M. E.; Cope, R. F.; Luciani, C. V.; Buser, J. Y. Small-volume continuous manufacturing of merestinib. Part 2. Technology transfer and cGMP manufacturing. *Org. Process Res. Dev.* **2019**, *23*, 870−881.

(7) McGlone, T.; Briggs, N. E. B.; Clark, C. A.; Brown, C. J.; Sefcik, J.; Florence, A. J. Oscillatory flow reactors (OFRs) for continuous manufacturing and crystallization. *Org. Process Res. Dev.* **2015**, *19*, 1186−1202.

(8) Ferguson, S.; Ortner, F.; Quon, J.; Peeva, L.; Livingston, A.; Trout, B. L.; Myerson, A. S. Use of continuous MSMPR crystallization with integrated nanofiltration membrane recycle for enhanced yield and purity in API crystallization. *Cryst. Growth Des.* **2014**, *14*, 617−627.

(9) Alvarez, A. J.; Myerson, A. S. Continuous plug flow crystallization of pharmaceutical compounds. *Cryst. Growth Des.* **2010**, *10*, 2219−2228.

(10) Powell, K. A.; Saleemi, A. N.; Rielly, C. D.; Nagy, Z. K. Periodic steady-state flow crystallization of a pharmaceutical drug using MSMPR operation. *Chem. Eng. Process.* **2015**, *97*, 195−212.

(11) Li, J.; Lai, T.-t. C.; Trout, B. L.; Myerson, A. S. Continuous crystallization of cyclosporine: Effect of operating conditions on yield and purity. *Cryst. Growth Des.* **2017**, *17*, 1000−1007.

(12) Quon, J. L.; Zhang, H.; Alvarez, A.; Evans, J.; Myerson, A. S.; Trout, B. L. Continuous crystallization of aliskiren hemifumarate. *Cryst. Growth Des.* **2012**, *12*, 3036−3044.

(13) Brown, C. J.; McGlone, T.; Yerdelen, S.; Srirambhatla, V.; Mabbott, F.; Gurung, R.; Briuglia, M. L.; Ahmed, B.; Polyzois, H.; McGinty, J. Enabling precision manufacturing of active pharmaceutical ingredients: workflow for seeded cooling continuous crystallisations. *Mol. Syst. Des. Eng.* **2018**, *3*, 518−549.

(14) Zhang, D.; Xu, S.; Du, S.; Wang, J.; Gong, J. Progress of pharmaceutical continuous crystallization. *Engineering* **2017**, *3*, 354−364.

(15) Lawton, S.; Steele, G.; Shering, P.; Zhao, L.; Laird, I.; Ni, X.-W. Continuous crystallization of pharmaceuticals using a continuous oscillatory baffled crystallizer. *Org. Process Res. Dev.* **2009**, *13*, 1357−1363.

(16) Wood, B.; Girard, K. P.; Polster, C. S.; Croker, D. M. Progress to date in the design and operation of continuous crystallization processes for pharmaceutical applications. *Org. Process Res. Dev.* **2019**, *23*, 122−144.

(17) Rohani, S.; Horne, S.; Murthy, K. Control of product quality in batch crystallization of pharmaceuticals and fine chemicals. Part 1: Design of the crystallization process and the effect of solvent. *Org. Process Res. Dev.* **2005**, *9*, 858−872.

(18) Bakar, M. R. A.; Nagy, Z. K.; Rielly, C. D. Seeded batch cooling crystallization with temperature cycling for the control of size uniformity and polymorphic purity of sulfathiazole crystals. *Org. Process Res. Dev.* **2009**, *13*, 1343−1356.

(19) Nagy, Z. K.; Fujiwara, M.; Braatz, R. D. Modelling and control of combined cooling and antisolvent crystallization processes. *J. Process Control* **2008**, *18*, 856−864.

(20) Van Eerdenbrugh, B.; Baird, J. A.; Taylor, L. S. Crystallization tendency of active pharmaceutical ingredients following rapid solvent evaporation—classification and comparison with crystallization tendency from under cooled melts. *J. Pharm. Sci.* **2010**, *99*, 3826−3838.

(21) Jiang, M.; Ni, X.-W. Reactive crystallization of paracetamol in a continuous oscillatory baffled reactor. *Org. Process Res. Dev.* **2019**, *23*, 882−890.

(22) Lindenberg, C.; Krättli, M.; Cornel, J.; Mazzotti, M.; Brozio, J. r. Design and optimization of a combined cooling/antisolvent crystallization process. *Cryst. Growth Des.* **2009**, *9*, 1124−1136.

(23) Durak, L.; Kennedy, M.; Langston, M.; Mitchell, C.; Morris, G.; Perlman, M. E.; Wendl, K.; Hicks, F.; Papageorgiou, C. D. Development and scale-up of a crystallization process to improve an API's physiochemical and bulk powder properties. *Org. Process Res. Dev.* **2018**, *22*, 296−305.

(24) Schenck, L.; Erdemir, D.; Saunders Gorka, L.; Merritt, J. M.; Marziano, I.; Ho, R.; Lee, M.; Bullard, J.; Boukerche, M.; Ferguson, S. Recent advances in co-processed APIs and proposals for enabling commercialization of these transformative technologies. *Mol. Pharmaceutics* **2020**, *17*, 2232−2244.

(25) Cote, A.; Erdemir, D.; Girard, K. P.; Green, D. A.; Lovette, M. A.; Sirota, E.; Nere, N. K. Perspectives on the Current State, Challenges, and Opportunities in Pharmaceutical Crystallization Process Development. *Cryst. Growth Des.* **2020**, *20*, 7568−7581.
(26) Ruecroft, G.; Hipkiss, D.; Ly, T.; Maxted, N.; Cains, P. W. Sonocrystallization: the use of ultrasound for improved industrial crystallization. *Org. Process Res. Dev.* **2005**, *9*, 923−932.
(27) Price, C. J. Application of Ultrasound in Crystallization (Sonocrystallization). *Engineering Crystallography: From Molecule to Crystal to Functional Form*; Springer, 2017; pp 301−313.
(28) Sander, J. R. G.; Zeiger, B. W.; Suslick, K. S. Sonocrystallization and sonofragmentation. *Ultrason. Sonochem.* **2014**, *21*, 1908−1915.
(29) Zhang, Z.; Sun, D.-W.; Zhu, Z.; Cheng, L. Enhancement of crystallization processes by power ultrasound: current state-of-the-art and research advances. *Compr. Rev. Food Sci. Food Saf.* **2015**, *14*, 303−316.
(30) Capelo-Martínez, J.-L. *Ultrasound in Chemistry: Analytical Applications*; John Wiley & Sons, 2009.
(31) Hatkar, U. N.; Gogate, P. R. Process intensification of anti-solvent crystallization of salicylic acid using ultrasonic irradiations. *Chem. Eng. Process.* **2012**, *57*, 16−24.
(32) Jiang, M.; Papageorgiou, C. D.; Waetzig, J.; Hardy, A.; Langston, M.; Braatz, R. D. Indirect ultrasonication in continuous slug-flow crystallization. *Cryst. Growth Des.* **2015**, *15*, 2486−2492.
(33) Ahmed, B.; Brown, C. J.; McGlone, T.; Bowering, D. L.; Sefcik, J.; Florence, A. J. Engineering of acetaminophen particle attributes using a wet milling crystallisation platform. *Int. J. Pharm.* **2019**, *554*, 201−211.
(34) Agimelen, O. S.; Svoboda, V.; Ahmed, B.; Cardona, J.; Dziewierz, J.; Brown, C. J.; McGlone, T.; Cleary, A.; Tachtatzis, C.; Michie, C. Multi-sensor inline measurements of crystal size and shape distributions during high shear wet milling of crystal slurries. *Adv. Powder Technol.* **2018**, *29*, 2987−2995.
(35) Luciani, C. V.; Conder, E. W.; Seibert, K. D. Modeling-aided scale-up of high-shear rotor−stator wet milling for pharmaceutical applications. *Org. Process Res. Dev.* **2015**, *19*, 582−589.
(36) Meng, W.; Sirota, E.; Feng, H.; McMullen, J. P.; Codan, L.; Cote, A. S. Effective Control of Crystal Size via an Integrated Crystallization, Wet Milling, and Annealing Recirculation System. *Org. Process Res. Dev.* **2020**, *24*, 2639−2650.
(37) Salvatori, F.; Mazzotti, M. Manipulation of particle morphology by crystallization, milling, and heating cycles: experimental characterization. *Ind. Eng. Chem. Res.* **2018**, *57*, 15522−15533.
(38) Wilson, D.; Bunker, M.; Milne, D.; Jawor-Baczynska, A.; Powell, A.; Blyth, J.; Streather, D. Particle engineering of needle shaped crystals by wet milling and temperature cycling: Optimisation for roller compaction. *Powder Technol.* **2018**, *339*, 641−650.
(39) Rajagopalan, A. K.; Bötschi, S.; Morari, M.; Mazzotti, M. Feedback Control for the Size and Shape Evolution of Needle-like Crystals in Suspension. III. Wet Milling. *Cryst. Growth Des.* **2019**, *19*, 2845−2861.
(40) Köllges, T.; Vetter, T. Polymorph Selection and Process Intensification in a Continuous Crystallization−Milling Process: A Case Study on l-Glutamic Acid Crystallized from Water. *Org. Process Res. Dev.* **2019**, *23*, 361−374.
(41) Li, Y.; O'Shea, S.; Yin, Q.; Vetter, T. Polymorph selection by continuous crystallization in the presence of wet milling. *Cryst. Growth Des.* **2019**, *19*, 2259−2271.
(42) Köllges, T.; Vetter, T. Model-based analysis of continuous crystallization/reaction processes separating conglomerate forming enantiomers. *Cryst. Growth Des.* **2017**, *17*, 233−247.
(43) Kamahara, T.; Takasuga, M.; Tung, H. H.; Hanaki, K.; Fukunaka, T.; Izzo, B.; Nakada, J.; Yabuki, Y.; Kato, Y. Generation of fine pharmaceutical particles via controlled secondary nucleation under high shear environment during crystallization process development and scale-up. *Org. Process Res. Dev.* **2007**, *11*, 699−703.
(44) Harter, A.; Schenck, L.; Lee, I.; Cote, A. High-shear rotor−stator wet milling for drug substances: expanding capability with improved scalability. *Org. Process Res. Dev.* **2013**, *17*, 1335−1344.
(45) Yang, Y.; Song, L.; Zhang, Y.; Nagy, Z. K. Application of wet milling-based automated direct nucleation control in continuous cooling crystallization processes. *Ind. Eng. Chem. Res.* **2016**, *55*, 4987−4996.
(46) Acevedo, D.; Kamaraju, V. K.; Glennon, B.; Nagy, Z. K. Modeling and characterization of an in situ wet mill operation. *Org. Process Res. Dev.* **2017**, *21*, 1069−1079.
(47) Yang, Y.; Song, L.; Gao, T.; Nagy, Z. K. Integrated upstream and downstream application of wet milling with continuous mixed suspension mixed product removal crystallization. *Cryst. Growth Des.* **2015**, *15*, 5879−5885.
(48) Hou, G.; Power, G.; Barrett, M.; Glennon, B.; Morris, G.; Zhao, Y. Development and characterization of a single stage mixed-suspension, mixed-product-removal crystallization process with a novel transfer unit. *Cryst. Growth Des.* **2014**, *14*, 1782−1793.
(49) Lee, I. Rotor-stator milling of APIs-between the morphology and breakage of crystals. *Am. Pharm. Rev.* **2004**, *7*, 120−123.
(50) Engstrom, J.; Wang, C.; Lai, C.; Sweeney, J. Introduction of a new scaling approach for particle size reduction in toothed rotor-stator wet mills. *Int. J. Pharm.* **2013**, *456*, 261−268.
(51) Koswara, A.; Nagy, Z. K. Anti-fouling control of plug-flow crystallization via heating and cooling cycle. *IFAC-PapersOnLine* **2015**, *48*, 193−198.

NOTE ADDED AFTER ASAP PUBLICATION

This article published ASAP on September 1, 2021. Figure 3a has been updated and the corrected version was reposted on September 8, 2021.

https://doi.org/10.1021/acs.oprd.1c00209
Org. Process Res. Dev. 2021, 25, 2119−2132